Eur. Phys. J. C (2024) 84:1124
https://doi.org/10.1140/epjc/s10052-024-13482-2

THE EUROPEAN PHYSICAL JOURNAL C

Regular Article - Theoretical Physics

Search for single vector-like B quark production in hadronic final states at the LHC

Bingfang Yang[1,a], **Zejun Li**[1,b], **Xinglong Jia**[1,c], **Stefano Moretti**[2,3,d], **Liangliang Shang**[1,2,e]

[1] School of Physics, Henan Normal University, Xinxiang 453007, People's Republic of China
[2] Department of Physics and Astronomy, Uppsala University, Box 516, 751 20 Uppsala, Sweden
[3] School of Physics and Astronomy, University of Southampton, Highfield, Southampton SO17 1BJ, UK

Received: 21 August 2024 / Accepted: 9 October 2024

Abstract In this paper, we study the discovery potential of a Vector-Like B quark (VLB) via the process $pp \to B(\to bZ)j \to b(Z \to \nu_l \bar{\nu}_l)j$ at the Large Hadron Collider (LHC) with $\sqrt{s} = 14$ TeV. In the framework of a simplified model, we perform a scan over its parameter space and test its viability following a Monte Carlo analysis developed to include all production and decay dynamics. We use cut-and-count combined with Extreme Gradient Boosting (XGBoost) methods to classify the signal and background events in order to improve the efficiency of signal identification and background rejection. We find that this approach can reduce background events significantly while the signal retention rate is much higher than that of traditional methods, thereby improving the VLB discovery potential. We then calculate the exclusion and discovery capabilities for VLBs and find that the advantages of the cut-and-count plus XGBoost method especially lie in the high-mass region, i.e., $m_B > 1500$ GeV. We finally obtain the following LHC results in terms of the coupling and chiral structure of a singlet heavy VLB interactions: (i) for $g^* = 0.2$ and $R_L = 0$ with 3000 fb^{-1}, the B quark mass can be be excluded (discovered) up to 3000 GeV (2500 GeV); (ii) for $g^* = 0.2$ and $R_L = 0.5$ with 3000 fb^{-1}, the exclusion (discovery) region can reach up to 4750 GeV (4250 GeV).

1 Introduction

The gauge hierarchy problem [1] caused by the quadratic divergence of the Higgs mass is one of the unsolved problems in the Standard Model (SM) of particle physics. For the past few decades, solving this problem has become a guiding principle for establishing New Physics (NP) models. Amongst these, vector-like quarks (VLQs) are often introduced to alleviate this problem since an extra SM-like chiral fermion has been disfavored by the Higgs data collected at the Large Hadron Collider (LHC) [2,3]. VLQs are a type of hypothetical fermions with spin 1/2 and color-triplets, which left- and right-handed components transform with the same properties under the SM electro-weak (EW) symmetry group [4]. There are seven possible multiplets of VLQs, depending on how they couple to the SM quarks [5]. These are EW singlets $[(T), (B)]$, doublets $[(X, T), (T, B), (B, Y)]$ and triplets $[(X, T, B), (T, B, Y)]$, where the fields X, Y, T, B have charges $+5/3e$, $-4/3e$, $+2/3e$ and $-1/3e$, respectively. Moreover, VLQs can explain other anomalies observed in experiments [6], such as the W mass anomaly [7,8]. Many phenomenological analyses on VLQs have also been carried out [9–34]. While most such analyses where concerned with pair production of VLQs, as the limits on their masses grow stronger, single production of VLQs has also become of phenomenological interest [5,9–11,14,18,19,22,23,35–50]. In particular, in Ref. [40], the authors have studied single production of vector-like B quarks (VLBs) via the bZ channel with $Z \to l^+l^-$ at the LHC. Herein, we will complement that study as we will be dealing with the same production process via the bZ channel but with $Z \to \nu\bar{\nu}$, again at the LHC but also in the presence of the up-to-date constraint $m_B > 1500$ GeV.

In experiment, the ATLAS and CMS collaborations have implemented many analyses in the search for VLQs at the

[a] e-mail: yangbingfang@htu.edu.cn
[b] e-mail: lizejun@stu.htu.edu.cn
[c] e-mail: jiaxinglong@stu.htu.edu.cn
[d] e-mails: s.moretti@soton.ac.uk ; stefano.moretti@physics.uu.se
[e] e-mails: shangliangliang@htu.edu.cn; liangliang.shang@physics.uu.se (corresponding author)

Published online: 29 October 2024

LHC. For VLBs, which this work focuses on, the CMS collaboration has performed a search via pair production in the fully hadronic final state using Run 2 data with 138 fb^{-1} and set lower limits on the VLB mass equal to 1570 GeV for BR$(B \to bH) = 100\%$ and 1540 GeV for BR$(B \to bZ) = 100\%$ [51], i.e., in terms of VLB Branching Ratios (BRs). For the singlet case, BR$(B \to bH)$ =BR$(B \to bZ)$= 25% and BR$(B \to tW) = 50\%$, the lower limit on the VLB mass is set to about 1060 GeV. For the (B, Y) doublet case BR$(B \to bH)$ =BR$(B \to bZ) = 50\%$ and BR$(B \to tW) = 0\%$, the lower limit on the VLB mass is set to 1500 GeV. As intimated, although VLBs can be pair produced through strong interactions, the single production process through EW interactions becomes more important when VLBs are heavy, because of phase space effects. However, we also notice that the single VLQ production is model dependent, unlike the double VLQ one. The ATLAS collaboration has performed a search for VLB single production decaying to a Z boson and a Higgs boson using Run 2 data with 139 fb^{-1} [52]. For an isospin singlet VLB, the search has excluded values of the c_W coupling[1] greater than 0.45 for m_B between 1.0 and 1.2 TeV. For 1.2 TeV $< m_B <$ 2.0 TeV, c_W values in the range 0.5–0.65 have been excluded. For a VLB as part of a (B, Y) doublet, the smallest excluded c_Z coupling values range between 0.3 and 0.5 for 1.2 TeV $< m_B <$ 2.0 TeV.

The NP processes can be rare and only differ slightly from the SM yield, a fact which represents a great challenge for physicists when analyzing data. Furthermore, data collected by LHC experiments are complex and highly dimensional whereas traditional data analysis techniques use a sequence of boolean decisions followed by statistical analysis on the selected data, both of which are based on the distribution of a single observed quantity motivated by physics considerations, which is not easily extended to the required higher dimensions [54]. As a result, physicists have done a lot of work to explore the application of machine learning (ML), including deep learning (DL), in particle physics and have developed a series of useful tools [55–57]. From these studies, we can see that ML has a natural advantage in identifying signals, wherein the Extreme Gradient Boosting (XGBoost) [58] algorithm, stemming from boosted decision trees (BDTs), has a unique advantage in finding NP effects [59]. For these reasons, we will adopt a XGBoost algorithm to improve the discovery potential of VLBs at the LHC, targeting not only Run 3 datasets, i.e., with 300 fb^{-1} of luminosity, but also those of a future high-luminosity LHC (HL-LHC) [60], i.e., with 3000 fb^{-1} of luminosity.

We organize our paper as follows. In Sect. 2, we briefly describe the effective Lagrangian of the singlet VLB. In Sect. 3, we present the event generation and analysis of signal and backgrounds. In Sect. 4, we explore the exclusion and discovery potential at the (HL-) LHC. Finally, we summarize our results in Sect. 5.

2 The effective Lagrangian

In a simplified model including an $SU(2)$ singlet VLB, the Lagrangian that describes how the VLB couples to SM quarks and EW bosons can be expressed as follows [53][2]:

$$\begin{aligned}\mathcal{L}_B = \frac{g g^*}{\sqrt{2}} \Bigg\{ & \sqrt{\frac{R_L}{1+R_L}} \frac{1}{\sqrt{2}} \left[\bar{B}_L W^-_\mu \gamma^\mu u_L\right] \\ & + \sqrt{\frac{1}{1+R_L}} \frac{1}{\sqrt{2}} \left[\bar{B}_L W^-_\mu \gamma^\mu t_L\right] \\ & + \sqrt{\frac{R_L}{1+R_L}} \frac{1}{2\cos\theta_W} \left[\bar{B}_L Z_\mu \gamma^\mu d_L\right] \\ & + \sqrt{\frac{1}{1+R_L}} \frac{1}{2\cos\theta_W} \left[\bar{B}_L Z_\mu \gamma^\mu b_L\right] \\ & - \sqrt{\frac{R_L}{1+R_L}} \frac{m_B}{2m_W} \left[\bar{B}_R H d_L\right] \\ & - \sqrt{\frac{1}{1+R_L}} \frac{m_B}{2m_W} \left[\bar{B}_R H b_L\right] \Bigg\} \\ & + h.c. \end{aligned} \tag{1}$$

Here, g is the $SU(2)_L$ gauge coupling constant, g^* parameterizes the single VLB production in association with SM quarks whereas m_W is the mass of the W boson. Further, R_L is the rate of the VLB decaying into the first and the third generation quarks. The decay widths of the VLB into SM quarks can be estimated as:

$$\begin{aligned}\Gamma(B \to Z d_i) = & \frac{g^2 g^{*2} c^2_{d_i}}{512 m_Z^2 m_B^3 \cos^2\theta_W} \\ & \times \left(m_B^4 + m_{d_i}^4 + m_B^2 m_Z^2 - 2m_Z^4 + m_{d_i}^2(-2m_B^2 + m_Z^2)\right) \\ & \times \sqrt{m_{d_i}^4 + \left(m_B^2 - m_Z^2\right)^2 - 2m_{d_i}^2(m_B^2 + m_Z^2)},\end{aligned}$$

[1] Note that, following Ref. [52], c_W, c_Z, c_H represents the coupling constants for interactions between the VLB and W, Z and H bosons, respectively. For singlet B and $m_B > 1$ TeV, $c_W \approx \kappa$, $c_Z \approx \kappa/(\sqrt{2}\cos\theta_W)$, where θ_W is the Weinberg angle, and $c_H = m_B\kappa/(\sqrt{2}v)$, where v is the Higgs vacuum expectation value, defined as $v \equiv 2m_W/g_W$, with g_W representing the $SU(2)_L$ weak coupling. Here, κ corresponds to κ_B in Ref. [53], where $\zeta_i = 1$ and c_W and c_H do not contain the factor $g_W/2$. Finally, in our paper, κ corresponds to g^* when $R_L = 0$.

[2] In Ref. [53], the effective Lagrangian for a singlet VLB is not clearly specified, yet, it can be obtained by incorporating the coefficients for the singlet VLB from Eq. (3.2) in Ref. [53]. This Lagrangian is presented in the singlet VLB model of FeynRules [61]. However, there is a missing factor of $\sqrt{2}$ in the Lagrangian and the charge of W is also inaccurately described on the website [62]. Nevertheless, the provided codes are accurate, and we employed these in our work.

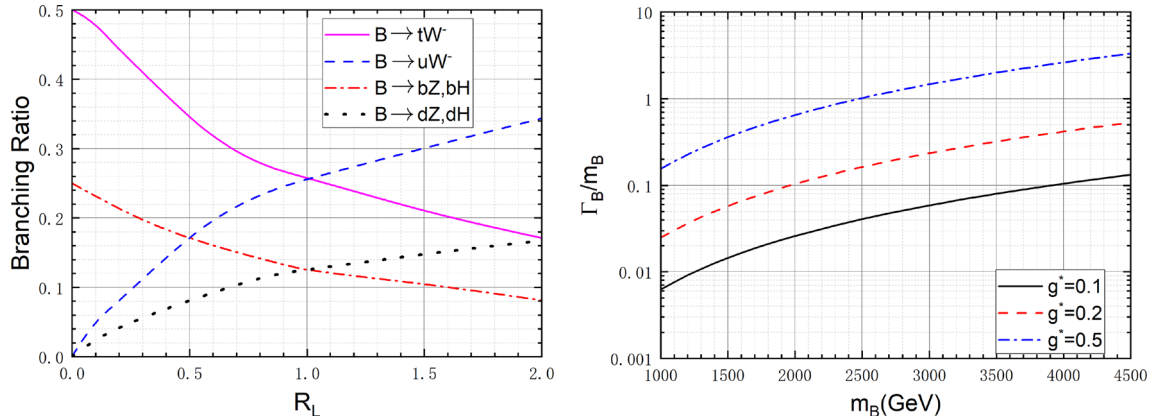

Fig. 1 The BRs of the VLB as a function of R_L with m_B=1500 GeV (left) and the width-to-mass ratios of the VLB as a function of m_B (right)

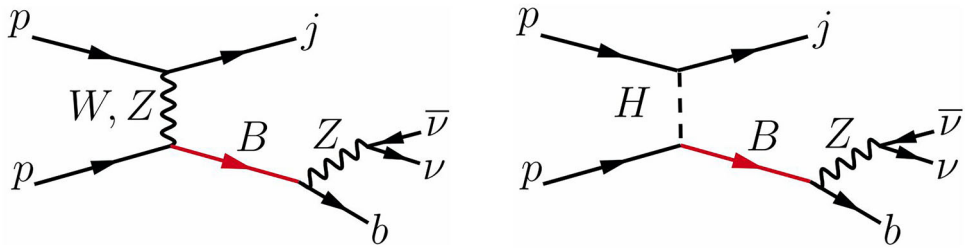

Fig. 2 Feynman diagrams for single VLB (in red) production with subsequent decay into bZ at the LHC

$$
\begin{aligned}
\Gamma(B \to W^- u_i) &= \frac{g^2 g^{*2} c_{u_i}^2}{256 m_W^2 m_B^3} \\
&\times \left(m_B^4 + m_{u_i}^4 + m_{u_i}^2 m_W^2 - 2m_W^4 + m_B^2(-2m_{u_i}^2 + m_W^2)\right) \\
&\times \sqrt{m_B^4 + \left(m_{u_i}^2 - m_W^2\right)^2 - 2m_B^2(m_{u_i}^2 + m_W^2)}, \\
\Gamma(B \to H d_i) &= \frac{g^2 g^{*2} c_{d_i}^2}{512 m_W^2 m_B} \left(m_B^2 + m_{d_i}^2 - m_H^2\right) \\
&\times \sqrt{m_{d_i}^4 + \left(m_B^2 - m_H^2\right)^2 - 2m_{d_i}^2 \left(m_B^2 + m_H^2\right)}\,. \qquad (2)
\end{aligned}
$$

Here, $i = 1, 3$ denotes the generation of SM quarks, $c_{d_i,u_i}^2 = R_L/(1+R_L)$ for $i = 1$, $c_{d_i,u_i}^2 = 1/(1+R_L)$ for $i = 3$. m_{u_i} and m_{d_i} are masses of the up-type and down-type SM quarks, respectively. Furthermore, m_H is the mass of the SM-like Higgs boson. If $R_L = 0$, the VLB is assumed to couple only to the third generation of SM quarks [5] and the Lagrangian can be simplified as:

$$
\begin{aligned}
\mathcal{L}_B = \frac{g g^*}{\sqrt{2}} \Bigg\{ &\frac{1}{\sqrt{2}} \left[\bar{B} W_\mu^- \gamma^\mu t_L\right] + \frac{1}{2\cos\theta_W} \left[\bar{B} Z_\mu^- \gamma^\mu b_L\right] \\
&- \frac{m_B}{2m_W} \left[\bar{B}_R H b_L\right] - \frac{m_B}{2m_W} \left[\bar{B}_L H b_R\right] \Bigg\} + h.c.
\end{aligned} \qquad (3)
$$

For $m_B > 1$ TeV, the decay BR of the VLB tends to be such that BR($B \to tW$):BR($B \to bZ$):BR($B \to bH$) = 2:1:1, as expected from the Goldstone equivalence theorem [63,64].

In Fig. 1, we show the BRs of our VLB as a function of R_L (left) for $m_B = 1500$ GeV and the width-to-mass ratios as a function of m_B (right). The BRs are independent of the coupling coefficient g^* whereas the width-to-mass ratios are approximately independent of R_L when $m_B > 1$ TeV. For a fixed g^*, the width-to-mass ratios are proportional to m_B^2. We can see that the VLB mainly decays to the third generation quarks for $R_L < 0.5$. However, when $R_L > 1$, the VLB decay to the first generation quarks gradually becomes the dominant decay mode. In this work, we primarily focus on the VLB coupling to the third generation quarks, hence, we consider two cases: $R_L = 0$ and $R_L = 0.5$. Since the constraints from the EW Precision Observables (EWPOs) on the coupling coefficient g^* are of $\mathcal{O}(10^{-1})$ [8], we consider here the range $g^* \leq 0.5$.

We explore the discovery potential of single VLB production through the channel $pp \to B(\to bZ)j \to b(Z \to \nu_l \bar{\nu}_l)j$, where b denotes the b-tagged jet and j stands for light-flavor jets. We show the typical Leading Order (LO) Feynman diagrams in Fig. 2. From this figure, we can see that the signal events are characterized by two jets with at least one b-tagged jet among these, along with significant missing (transverse) energy. Therefore, the primary SM backgrounds are $pp \to Zjjj$, $pp \to bZj$, $pp \to ZZ$ and $pp \to ZH$. Among these, $pp \to bZj$ is an irreducible background while the others are considered reducible backgrounds. The latter must be taken into account due to jets exhibiting lower tagging efficiencies and higher mistagging rates compared to leptons at hadron colliders. We have also evaluated further backgrounds including $pp \to W^\pm Z$ and determined that their impact can be disregarded according to the selection criteria that will be discussed later.

We calculate the LO cross sections of the signal process by MadGraph5_aMC@NLO [65] with the NNPDF23NLO

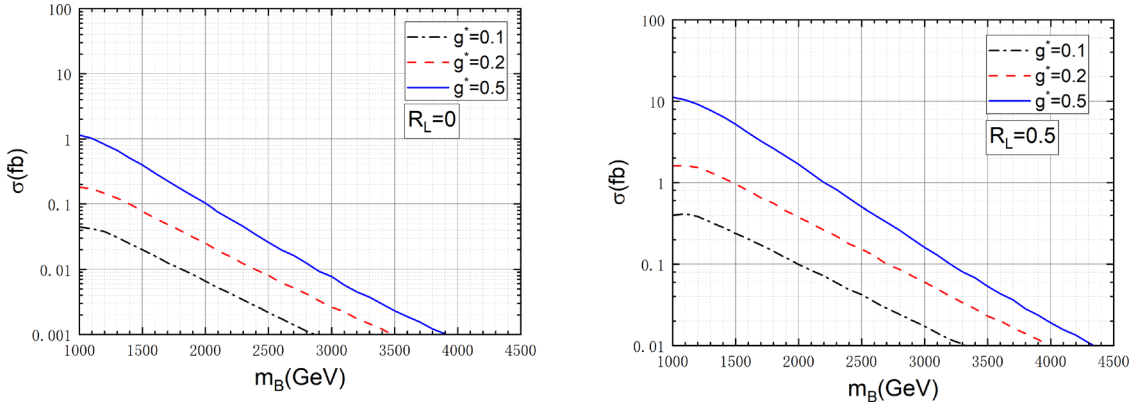

Fig. 3 Cross sections of the signal process $pp \to B(\to bZ)j \to b(Z \to \nu_l \bar{\nu}_l)j$ as a function of m_B at the 14 TeV LHC with $g^* = 0.1, 0.2, 0.5$ for R_L=0 (left) and R_L=0.5 (right). Here, the conjugate processes have been included

Parton Distribution Functions (PDFs) [66] and default renormalization and factorization scales. The cross sections at 14 TeV LHC are depicted as a function of m_B in Fig. 3, where we take $g^* = 0.1$, 0.2 and 0.5 as well as $R_L = 0$ and 0.5 as examples. The input SM parameters are taken as follows[3] [67]:

$$m_b = 4.18\ \text{GeV}, \quad m_Z = 91.1876\ \text{GeV},$$
$$m_H = 125.25\ \text{GeV},$$
$$G_F = 1.166378 \times 10^{-5}\ \text{GeV}^{-2}, \quad \sin^2\theta_W = 0.231,$$
$$\alpha_{\text{EM}}(m_Z) = 1/128.$$

From Fig. 3, we can see that the signal cross sections decrease rapidly with increasing m_B. For a fixed m_B, the cross sections increase rapidly with increasing g^* due to $\sigma \propto g^{*2}$. Furthermore, for equivalent values of the coupling g^* and the mass m_B, the cross section for $R_L = 0.5$ is larger than that for $R_L = 0$. This is because the former scenario involves B mixing with the first generation quarks, which significantly enlarges the single VLB production rate due to the increased sea quark PDFs. However, we limit ourselves to studying cases where $R_L < 0.5$ because there are stringent constraints from non-LHC flavor physics data on VLQs mixing significantly with lighter quarks [68–78]. We list the LO cross sections and the K factors representing the QCD corrections for the background processes in Table 1.

3 Event generation and analysis

We conduct a detailed detector simulation in this work. The signal model file is obtained from FeynRules [81] and, again, parton-level events are generated using MadGraph 5_aMC@NLO with the NNPDF23NLO PDF set. Indeed, the factorization and renormalization scales are still set to their default values in MadGraph5_aMC@NLO.

These events are then input into Pythia 8.3 [82] for parton showering and hadronization. Subsequently, fast detector simulations are performed using Delphes 3.4.2 [83] with the built-in detector configurations of the LHC Run 3 and HL-LHC [84]. Jets are clustered using FastJet [85] employing the anti-kt algorithm [86]. Settings for the cone radius of the jet tagging algorithm and isolated leptons are implemented in Delphes with default values. Then, both signal and background events are analyzed using MadAnalysis 5 [87]. Finally, we scan the VLB parameter space and connect these programs with the help of the EasyScan_HEP package [88]. To quantify the observability of the signal, we utilize the following formula to calculate the expected discovery and exclusion significance, without considering systematic uncertainties for simplicity [89]:

$$\mathcal{Z}_{\text{disc}} = \sqrt{2\left[(s+b)\ln\left(1+\frac{s}{b}\right) - s\right]}, \tag{4}$$

and

$$\mathcal{Z}_{\text{excl}} = \sqrt{2\left[s - b\ln\left(1+\frac{s}{b}\right)\right]}, \tag{5}$$

where s and b are the number of signal (s) and total background (b) events, respectively, after applying the selection criteria that will be discussed later. The exclusion significance is denoted by $\mathcal{Z}_{\text{excl}} = 2$ whereas the discovery significance is denoted by $\mathcal{Z}_{\text{disc}} = 5$.

To accommodate contributions from higher-order QCD corrections, we adjust the cross sections of the dominant backgrounds from the LO to the Next-to-LO (NLO) or Next-to-NLO (NNLO) using K factors, as detailed in Table 1. We assume that kinematic distributions are minimally impacted by these higher-order effects. Therefore, for simplicity, we

[3] Here, m_W is calculated as $\sqrt{\frac{M_Z^2}{2} + \sqrt{\frac{M_Z^4}{4} - \frac{\alpha_{\text{EW}}\pi M_Z^2}{G_F\sqrt{2}}}}$ within MadGraph5_aMC@NLO.

Table 1 The LO cross sections and the K factors representing the QCD corrections for the background processes at the 14 TeV LHC. Here, the cross section of bZj includes the contribution from the conjugate process of $pp \to \bar{b}Zj$

Processes	$Zjjj$	bZj	ZZ	ZH
$\sigma_{\rm LO}$ (fb)	22.5	5.8	0.1	0.1
K factor	1.2 [65]	1.2 [79]	1.8 [80]	1.3 [65]

scale the kinematic distributions, which we will discuss later, using constant bin-independent K factors. It is then worth noting that, for the signal, we maintain the LO cross section, ensuring that the exclusion and discovery potentials depicted in this analysis remain conservative. The inclusion of higher-order QCD corrections could indeed bolster these potentials.

For our analysis, we establish as reference values for the couplings $g^* = 0.2$ and $R_L = 0$. Furthermore, along the VLB mass direction, our benchmark points (BPs) are located at the m_B values of 1500 GeV and 2000 GeV. However, we will later showcase the excluded 2σ and 5σ discovery thresholds in the $g^* - m_B$ plane, considering two different values of R_L, namely 0 and 0.5 and more finely sifted m_B values.

Due to the large mass of the VLB, its decay products are highly boosted, this resulting in the transverse momentum (p_T) peaks of the signals being larger than those of the (SM) backgrounds. In Fig. 4, we present several differential distributions for signals and backgrounds at the LHC, including the transverse momentum spectrum of the leading b-tagged jet ($p_T^{b_1}$), the distribution of total transverse hadronic energy H_T (defined as $H_T \equiv \sum_{\text{hadronic particles}} |\mathbf{p}_T|$) and the that of the missing transverse energy $\not{E}_T$. Additionally, the signal process involves an outgoing light quark, leading to a light-flavor forward jet within the detector. Therefore, we also display kinematic distributions showcasing distinct spatial characteristics, such as the pseudorapidity distribution of the leading light-flavor jet η_{j_1} and the distribution of spatial separation ΔR between the leading b-tagged jet and the leading light-flavor jet. The spatial separation is defined as $\Delta R = \sqrt{\Delta\Phi^2 + \Delta\eta^2}$, representing the separation in the rapidity (η)-azimuth (ϕ) plane.

Then, we employ the XGBoost algorithm to enhance the discovery potential of the VLB at the LHC. We select four signal BPs with m_B values of 1500 GeV, 2000 GeV, 3000 GeV and 4000 GeV while fixing $g^* = 0.1$ and $R_L = 0$ throughout, as kinematic distributions are minimally affected by the coupling g^* and the mixing parameter R_L. The background events are generated for the following processes here:

- $pp \to Z(\to \nu_l \bar{\nu}_l) jjj$,
- $pp \to bZ(\to \nu_l \bar{\nu}_l) j$,
- $pp \to Z(\to \nu_l \bar{\nu}_l) Z(\to b\bar{b}/jj)$,
- $pp \to Z(\to \nu_l \bar{\nu}_l) H(\to b\bar{b})$.

Considering the characteristics of the signal distributions, for the purpose of optimising the Monte Carlo (MC) generation efficiency, events in this analysis must satisfy $p_T^{j,b} > 200$ GeV and $\not{E}_T > 400$ GeV at the parton level,[4] implemented using MadGraph5_aMC@NLO, and $N(j) \geq 1$ and $N(b) \geq 1$ at the detector level, implemented using MadAnalysis 5.

Each event from the signal BPs and the four types of backgrounds corresponds to a 10-dimensional event vector constructed by 9-dimensional input features and a 1-dimensional target variable. The input features consist of the number of b-tagged jets $N(b)$, the number of light-flavor jets $N(j)$, the transverse momentum ($p_T^{b_1}$) and pseudorapidity (η_{b_1}) of the leading b-tagged jet, the transverse momentum ($p_T^{j_1}$) and pseudorapidity (η_{j_1}) of the leading light-flavor jet, the spatial separation between the leading b-jet and light-jet $\Delta R(b_1, j_1)$, the total transverse hadronic energy H_T and the missing energy $\not{E}_T$, obtained with the assistance of expert mode in MadAnalysis 5. The target variable is set as 1 for signal events and 0 for background events. We employ 8×10^5 event vectors, with equal contributions from each signal BP and background process, as training data. This dataset enables the XGBoost model (hereafter referred to as the X-model) to learn the relationships between features and how to map these onto target variables. Additionally, we use 1.6×10^4 event vectors, with equal contributions from each signal BP and background process, as testing data to evaluate the performance of the trained X-model on new signal and background events different from those in the training data.

There are hyperparameters used to fine-tune the performance of the X-model. The learning rate α controls the step size during the minimization of a logistic loss function $\mathcal{F}$:

$$\mathcal{F} = -\frac{1}{N}\sum_{i=1}^{N} [y_i \ln(p_i) + (1 - y_i)\ln(1 - p_i)]\,. \tag{6}$$

Here, N represents the number of events used to train the X-model, y_i denotes the target variable for each event and p_i indicates the predicted probability of the signal class for the i-th event. The fractions of event vectors ($r_{\rm s}$) and features ($r_{\rm f}$) in each event vector can be randomly selected for each tree. This randomness is introduced into the X-model

[4] We have indeed checked that these are not biasing the detector level events, see Cut-2 and -4 below.

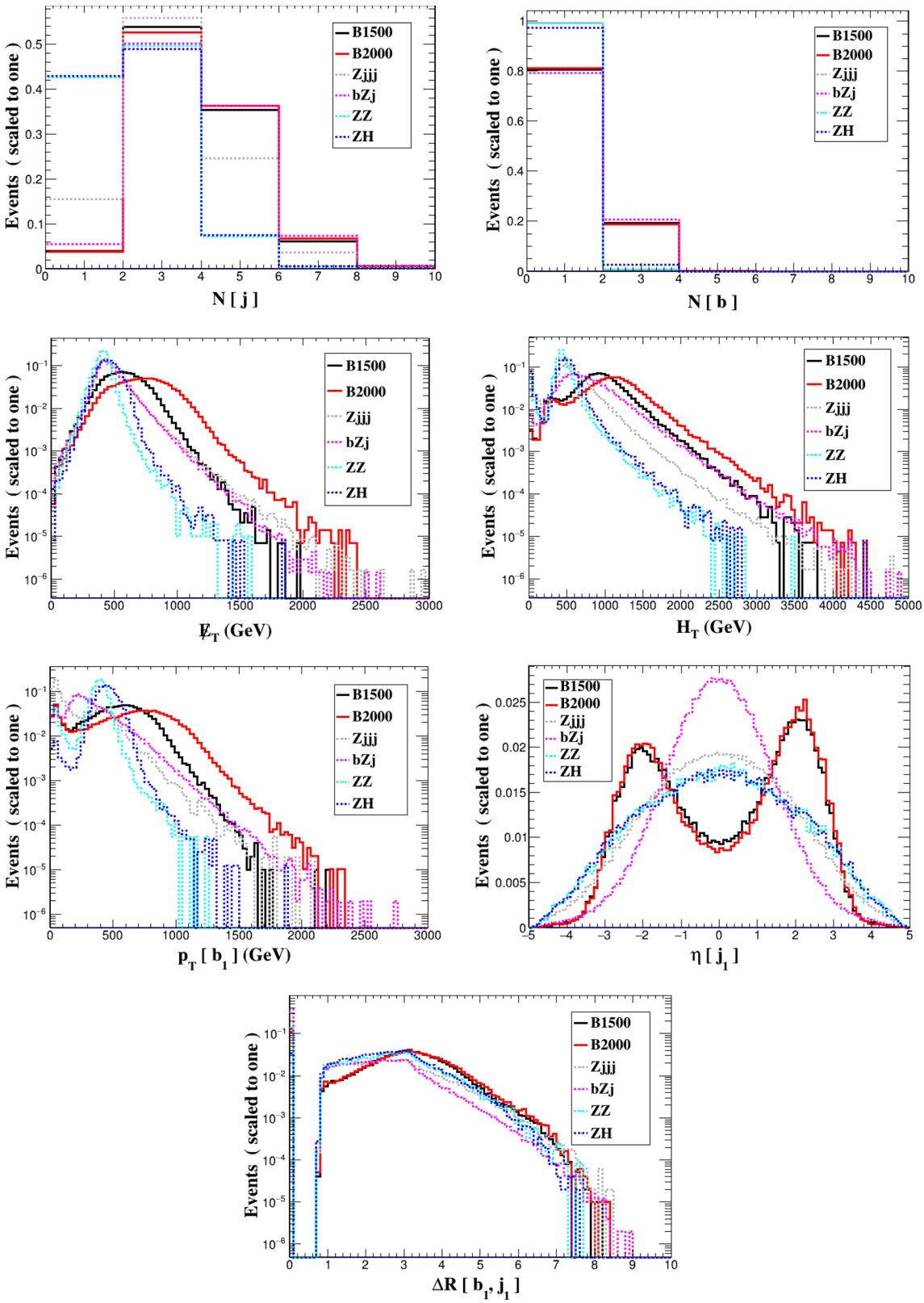

Fig. 4 Normalized distributions for the signals ($m_B = 1500$ GeV and 2000 GeV are selected as examples) and backgrounds at the 14 TeV LHC for $g^* = 0.2$ and $R_L = 0$

Table 2 The hyperparameter ranges and optimal values considered in this work

Hyperparameter	α	γ	n_t	n_d	r_s	r_f
Range	[0.01, 0.3]	[1, 5]	[20, 201]	[3, 21]	[0.5, 1]	[0.5, 1]
Optimal value	0.2	1.3	183	15	0.96	0.99

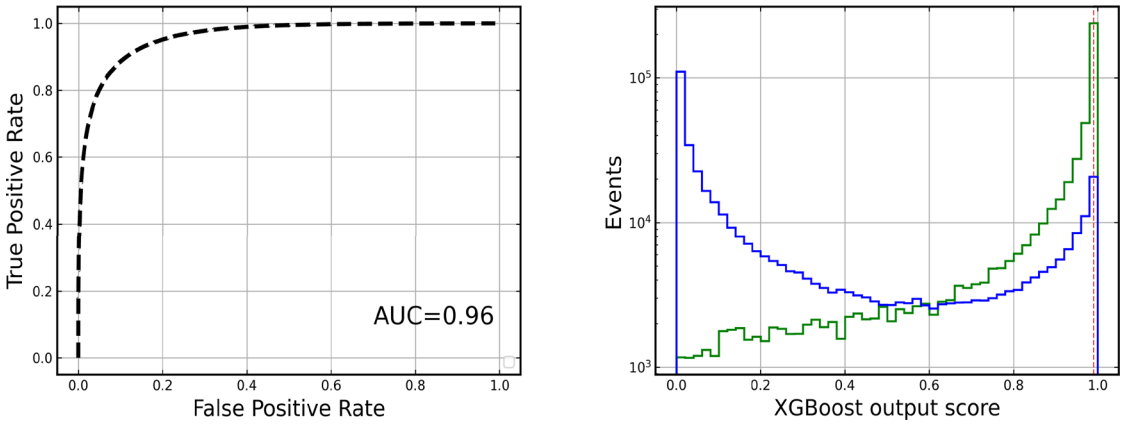

Fig. 5 Model performance on testing data. The left is the ROC curve while AUC represents the area under the curve. The right is the score distributions relevant to testing data. The green line stands for the signal while the blue line stands for all the backgrounds. The vertical red line stands for the threshold we choose

to enhance its generality. Additionally, the parameter γ prevents overfitting by penalizing excessively large and deep trees. If $\mathcal{F} > \gamma$, a further partition on a leaf node of the tree is required. We specify the learning rate to range between 0.01 and 0.5. The ranges for the fractions of event vectors and features are established as $r_{s,f} \in [0.5, 1.0]$. Furthermore, the ranges for the number of trees n_t and the maximum depth of each tree n_d are set as [50, 201] and [3, 21], respectively. A summary of these hyperparameter ranges and the optimal set of hyperparameters is provided in Table 2.

When assessing the performance of a set of hyperparameters, each p_i and p_{i+1} serves as threshold probabilities denoted by $\mathcal{T}_j$ ($j = 1, \ldots, N+1$). For every $\mathcal{T}_j$, if $p_i > \mathcal{T}_j$ ($i = 1, \ldots, N$), the corresponding event is classified as a signal, otherwise, it is classified as background. Consequently, each set of hyperparameters is associated with a receiver operating characteristic (ROC) curve, which illustrates the true positive rate (TPR) against the false positive rate (FPR) at various threshold settings. Here, j ranges from 1 to $N+1$ and the area under the ROC curve (AUC) [90] determines the effectiveness of the hyperparameters. Bayesian optimization, as introduced by [91], is employed to discover the optimal set of hyperparameters for this study. The objective function chosen for this optimization is the AUC value. During each iteration of Bayesian optimization, the training event vectors are randomly split into a 4:1 ratio. The former portion is utilized to train the X-model using XGBoost, while the latter is reserved for guiding the selection of the next set of hyperparameters to evaluate via Bayesian optimization. Subsequently, the optimal set of hyperparameters is identified based on maximizing the AUC value. Once this optimal set is determined, it represents the desired configuration for the X-model, which we refer to as the trained X-model. The trained X-model is then applied to the testing data as discussed earlier. Subsequently, the threshold probability closest to the point (1,0) on the resulting ROC curve is used as the selection criterion of the XGBoost algorithm to distinguish signal from background events used to achieve discovery or exclusion. We denote this threshold probability as $\mathcal{T}^*$. Ultimately, we utilize the trained X-model to generate the ROC curve and probability distributions of X-model outputs for events in the testing data. These plots, along with the selection criterion $\mathcal{T}^*$, are depicted in Fig. 5.

4 LHC exclusion and discovery potential

Drawing from the kinematic distributions illustrated in Fig. 4, we implement the subsequent kinematic selection criteria on the events to distinguish the signal from the backgrounds:

Cut-1 There are at least two jets ($N(j, b) \geq 2$) and at least one b-tagged jet among these ($N(b) \geq 1$).

Table 3 Cut flow of the cross sections (in fb) for the signals with two typical VLB quark masses and backgrounds at the 14 TeV LHC using the cut-and-count method. Here we take the parameters $g^* = 0.2$ and $R_L = 0$

Cuts	Signals		Backgrounds			
	1500 GeV	2000 GeV	$Zjjj$	bZj	ZZ	ZH
Initial	0.079	0.024	26.94	6.26	0.14	0.11
Cut-1	0.056	0.017	2.26	4.55	0.017	0.046
Cut-2	0.030	0.011	0.24	0.77	0.0009	0.013
Cut-3	0.015	0.006	0.07	0.13	0.0002	0.0046
Cut-4	0.010	0.005	0.02	0.04	4.26×10^{-6}	0.0001
Efficiency	12.9%	20.8%	7.4×10^{-4}	6.8×10^{-3}	3.0×10^{-5}	9.0×10^{-4}

Table 4 Cut flow of the cross sections (in fb) for the signals with two typical VLB quark masses and backgrounds at the 14 TeV LHC using the XGBoost method. Here we take the parameters $g^* = 0.2$ and $R_L = 0$

Cuts	Signals		Backgrounds			
	1500 GeV	2000 GeV	$Zjjj$	bZj	ZZ	ZH
Initial	0.079	0.024	26.94	6.26	0.14	0.11
Basic cuts	0.056	0.017	2.26	4.55	0.017	0.046
$\mathcal{T}^*$	0.006	0.005	0.0075	0.019	0.000005	0.00002
Efficiency	7.5%	20.8%	2.8×10^{-4}	3.0×10^{-3}	3.6×10^{-5}	1.8×10^{-4}

Cut-2 The transverse momentum of the leading b-tagged jet is required to be greater than 500 GeV ($p_T^{b_1} > 500$ GeV).

Cut-3 The pseudorapidity of the leading light-flavor jet is required to be greater than 1.8 ($|\eta_{j_1}| > 1.8$). Additionally, the spatial separation between the leading b-tagged jet and the leading light-flavor jet is required to be greater than 2.0 to reduce background from the process $pp \to bZj$, which contains the b quark in the initial state ($\Delta R(j_1, b_1) > 2.0$).

Cut-4 The total transverse hadronic energy is required to be greater than 800 GeV ($H_T > 800$ GeV) and the transverse missing energy is required to be greater than 500 GeV ($\not{E}_T > 500$ GeV).

We present the cross sections of two representative signals, with m_B values set at 1500 GeV and 2000 GeV, along with the corresponding backgrounds. These are depicted after applying the selection criteria detailed in Tables 3 and 4 for the cut-and-count method and XGBoost method, respectively. To construct these tables, we have simulated 10^5 events at the detector level for each signal and background process.

From Table 3, we can see that, among the four types of backgrounds, the dominant ones are the $Zjjj$ and bZj prior to any cuts. The first two cuts, pertaining to the number of final jets and transverse momentum of the leading b-tagged jets, significantly cut events from $Zjjj$ and ZZ, achieving a cumulative reduction rate of approximately 99%. Subsequently, the third cut, addressing pseudorapidities and spatial separations, efficiently cuts bZj events with a reduction rate of about 83%. Furthermore, imposing stringent requirements on H_T and $\not{E}_T$ successfully cuts overall around 70% of background events while retaining 70% of signal ones. Altogether, at the end of the cut flow, all backgrounds undergo notable suppression whereas the signals maintain a relatively favorable efficiency. In the end, the primary background contributions originate from the $Zjjj$ and bZj SM processes, which remain comparable in magnitude to the signal remnants, exhibiting cross sections of 0.02 fb and 0.04 fb, respectively. Finally, compared to the cut-and-count method, from Table 4, we can see that the signal significance is clearly improved further by the XBoost method.

To determine the exclusion and discovery reach at the 14 TeV LHC, using the two methods adopted here (i.e., the traditional cut-and-count one and the ML one), we perform calculations spanning the interval $m_B = 1500$ GeV to 3000 GeV. BPs are now selected at intervals of 250 GeV in the VLB mass, with $R_L = 0$ and $g^* = 0.2$. For each signal BP, we simulate 10^5 events, while for each background, we simulate 10^6 events. It has been verified that different values of R_L and g^* yield the same efficiency when m_B remains constant.

In Fig. 6, we show the 2σ (exclusion) and 5σ (discovery) lines on the $g^* - m_B$ plane for $R_L = 0$ at the 14 TeV LHC. We can see that VLBs can be excluded in the regions of $g^* \in [0.35, 0.50]$ and $m_B \in [1500\text{ GeV}, 2300\text{ GeV}]$ assuming an integrated luminosity of 300 fb^{-1} (Run 3). With a value for the latter of 3000 fb^{-1} (HL-LHC), instead, the exclusion

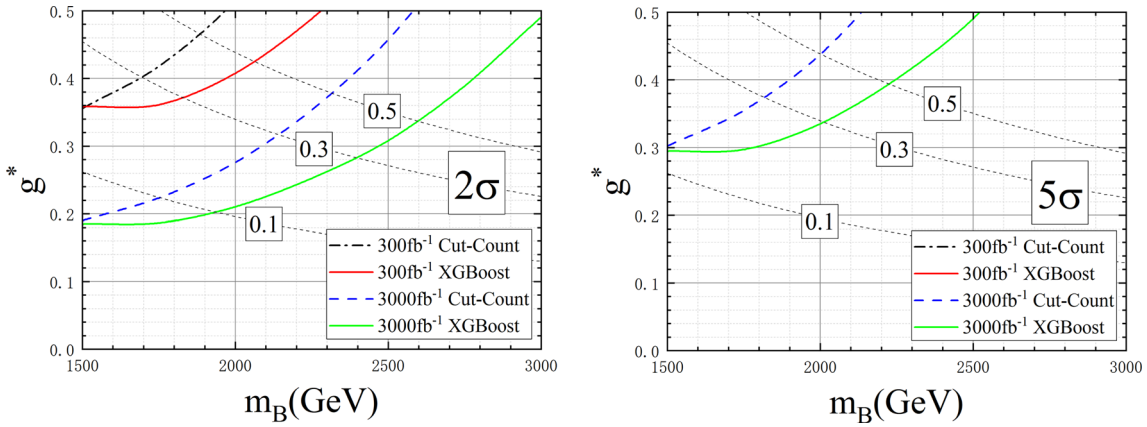

Fig. 6 Exclusion (left) and discovery (right) potential for the VLB signal on the $g^* - m_B$ planes for $R_L = 0$ at the 14 TeV LHC, considering the two methods adopted in our analysis. Three typical luminosities, 300 fb^{-1}, 1000 fb^{-1} and 3000 fb^{-1}, are illustrated. The dashed lines denote the width-to-mass ratios Γ_B/m_B

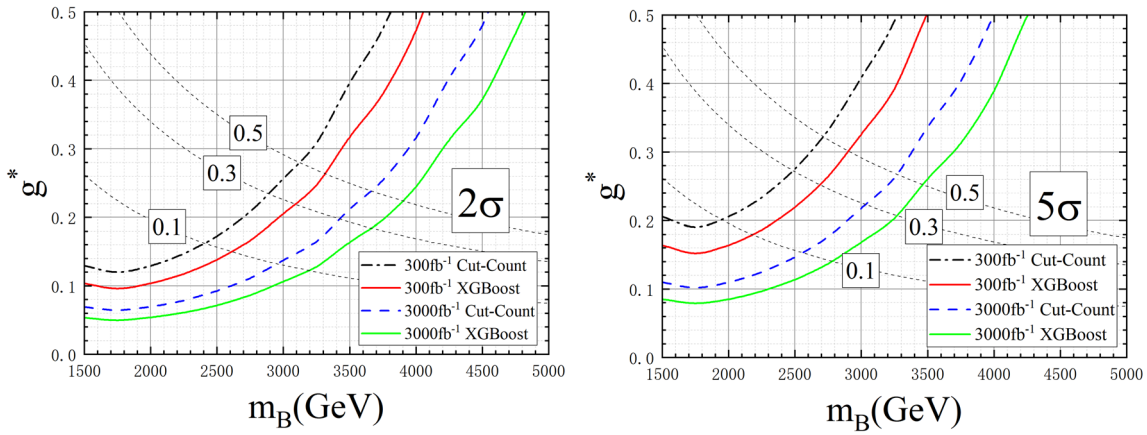

Fig. 7 Same as Fig. 6, but for $R_L = 0.5$

regions can be extended to $g^* \in [0.18, 0.50]$ and $m_B \in [1500\ \text{GeV}, 3000\ \text{GeV}]$. Accordingly, the discovery regions are $g^* \in [0.30, 0.50]$ and $m_B \in [1500\ \text{GeV}, 2500\ \text{GeV}]$.

Figure 7 is the same as Fig. 6, but for $R_L = 0.5$. We can see that the exclusion regions are $g^* \in [0.10, 0.50]$ and $m_B \in [1500\ \text{GeV}, 4050\ \text{GeV}]$ with 300 fb^{-1}, which can be extended to $g^* \in [0.05, 0.50]$ and $m_B \in [1500\ \text{GeV}, 4750\ \text{GeV}]$ with 3000 fb^{-1}. The discovery regions are $g^* \in [0.16, 0.50]$ and $m_B \in [1500\ \text{GeV}, 3500\ \text{GeV}]$ with 300 fb^{-1} plus $g^* \in [0.08, 0.50]$ and $m_B \in [1500\ \text{GeV}, 4250\ \text{GeV}]$ with 3000 fb^{-1}.

5 Summary

In this work, we have utilized a simplified model approach to test the exclusion and discovery potential of a VLB signal at both the current LHC (Run 3) and a future HL-LHC. We have employed both a standard cut-and-count method and a ML based XGBoost algorithm to achieve this goal. Specifically, we have focused on the process $pp \to B(\to bZ)j \to b(Z \to \nu_l \bar{\nu}_l)j$ as signal.

Initially, we have generated signal and background events using state-of-the-art computing tools. Subsequently, we have applied the cut-and-count method and the XGBoost algorithm to classify these events, effectively distinguishing between signal and background. For the XGBoost approach, we have trained the ML model using MC data and utilized Bayesian optimization to determine the optimal combination of hyperparameters. We have then employed this trained model to classify events and determine cut efficiencies via selection thresholds. Finally, we have evaluated the exclusion and discovery capabilities of the signal over both reducible and irreducible backgrounds across different LHC luminosities (and fixed $\sqrt{s} = 14$ TeV).

Our analysis has revealed significant sensitivities to this VLB process across various LHC stages, spanning from current to future machine configurations. These appear to

Table 5 Comparison of exclusion and discovery capabilities of different VLB signals with $\sqrt{s} = 14$ TeV and $\mathcal{L} = 3000$ fb^{-1} from different works

LHC	Decay	Exclusion		Discovery		References
		g^*	m_B (GeV)	g^*	m_B (GeV)	
$R_L = 0$	$B \to tW$	[0.2,0.5]	[1800,2400]	[0.3,0.5]	[1750,2100]	[38]
$R_L = 0$	$B \to bZ$	[0.2,0.5]	[1300,1800]	[0.3,0.5]	[1300,1500]	[40]
$R_L = 0$	$B \to bZ$	[0.2,0.5]	[1500,3000]	[0.3,0.5]	[1500,2500]	this work
R_L=0.5	$B \to bZ$	[0.2,0.5]	[3750,4750]	[0.3,0.5]	[3700,4250]	this work

improve significantly upon more traditional methods used in phenomenological analyses.

Indeed, for comparison, we finish by listing previous results on searching for a VLB at the HL-LHC in Table 5, also including $B \to tW$ decays, against ours. Since the advantages of XGBoost method lie in the high-mass region, we focus for this comparison over the region $m_B > 1500$ GeV. (Recall that the VLB coupling strength g^* is also described as κ_B in other references and their relation is $g^* = \kappa_B$ [53].) By comparing these results, we can see that the XGBoost algorithm does improve significantly the sensitivity of searches for a VLB with the same luminosity, a result which makes the exploration of VLB signals ever more promising also from the experimental side. However, it should be noted that, due to the inherent characteristics of the ML algorithm, certain limits to its applicability exist. For instance, when the mass of the VLB greatly exceeds the upper bound of the training set (in this work, 4000 GeV), the predictive capability of the model significantly diminishes. In forthcoming research, our primary focus will be on enhancing the model to address this issue.

Acknowledgements We thank Luca Panizzi for helpful discussions.

Funding This work of BY, ZL, XJ and LS is supported by the Natural Science Foundation of Henan Province under Grant No. 232300421217, the National Research Project Cultivation Foundation of Henan Normal University under Grant No. 2021PL10, the China Scholarship Council under Grant No. 202208410277 and also powered by the High Performance Computing Center of Henan Normal University. The work of SM is supported in part through the NExT Institute, the Knut and Alice Wallenberg Foundation under the Grant No. KAW 2017.0100 (SHIFT) and the STFC Consolidated Grant No. ST/L000296/1.

Data Availability Statement Data will be made available on reasonable request. [Authors' comment: The datasets generated during and/or analysed during the current study are available from the corresponding author on reasonable request].

Code Availability Statement Code/software will be made available on reasonable request. [Authors' comment: The code/software generated during and/or analysed during the current study is available from the corresponding author on reasonable request].

Funded by SCOAP^3.

References

1. K.G. Wilson, The renormalization group and strong interactions. Phys. Rev. D **3**, 1818 (1971). https://doi.org/10.1103/PhysRevD.3.1818
2. ATLAS Collaboration, G. Aad et al., Combined measurements of Higgs boson production and decay using up to 80 fb^{-1} of proton-proton collision data at $\sqrt{s} = 13$ TeV collected with the ATLAS experiment. Phys. Rev. D **101**(1), 012002 (2020). https://doi.org/10.1103/PhysRevD.101.012002. arXiv:1909.02845 [hep-ex]
3. C.M.S. Collaboration, A.M. Sirunyan et al., Measurement and interpretation of differential cross sections for Higgs boson production at $\sqrt{s} = 13$ TeV. Phys. Lett. B **792**, 369–396 (2019). https://doi.org/10.1016/j.physletb.2019.03.059. arXiv:1812.06504 [hep-ex]
4. A. De Simone, O. Matsedonskyi, R. Rattazzi, A. Wulzer, A first top partner hunter's guide. JHEP **04**, 004 (2013). https://doi.org/10.1007/JHEP04(2013)004. arXiv:1211.5663 [hep-ph]
5. J.A. Aguilar-Saavedra, R. Benbrik, S. Heinemeyer, M. Pérez-Victoria, Handbook of vectorlike quarks: mixing and single production. Phys. Rev. D **88**(9), 094010 (2013). https://doi.org/10.1103/PhysRevD.88.094010. arXiv:1306.0572 [hep-ph]
6. G.C. Branco, M.N. Rebelo, Vector-like quarks. PoS **DISCRETE2020-2021**, 004 (2022). https://doi.org/10.22323/1.405.0004. arXiv:2208.07235 [hep-ph]
7. S.P. He, Leptoquark and vector-like quark extended model for simultaneous explanation of W boson mass and muon g–2 anomalies*. Chin. Phys. C **47**(4), 043102 (2023). https://doi.org/10.1088/1674-1137/ac9e4c. arXiv:2205.02088 [hep-ph]
8. J.J. Cao, M. L., L.L. Shang, S.Y. Wang, B.F. Yang, Interpreting the W-mass anomaly in vectorlike quark models. Phys. Rev. D **106**(5), 055042 (2022). https://doi.org/10.1103/PhysRevD.106.055042. arXiv:2204.09477 [hep-ph]
9. N. Vignaroli, Discovering the composite Higgs through the decay of a heavy fermion. JHEP **07**, 158 (2012). https://doi.org/10.1007/JHEP07(2012)158. arXiv:1204.0468 [hep-ph]
10. N. Vignaroli, Early discovery of top partners and test of the Higgs nature. Phys. Rev. D **86**, 075017 (2012). https://doi.org/10.1103/PhysRevD.86.075017. arXiv:1207.0830 [hep-ph]

11. B.F. Yang, B.F. Hou, H.Y. Zhang, N. Liu, Single production of vectorlike top partner decaying to Wb in the leptonic channel at ep colliders in the littlest Higgs model with T-parity. Phys. Rev. D **99**(9), 095002 (2019). https://doi.org/10.1103/PhysRevD.99.095002. arXiv:1904.07434 [hep-ph]
12. N. Liu, L. Wu, B.F. Yang, M.C. Zhang, Single top partner production in the Higgs to diphoton channel in the Littlest Higgs Model with T-parity. Phys. Lett. B **753**, 664–669 (2016). https://doi.org/10.1016/j.physletb.2015.12.066. arXiv:1508.07116 [hep-ph]
13. J. Nutter, R. Schwienhorst, D.G.E. Walker, J. Yu, Single top production as a probe of B' quarks. Phys. Rev. D **86**, 094006 (2012). https://doi.org/10.1103/PhysRevD.86.094006. arXiv:1207.5179 [hep-ph]
14. A. Deandrea, T. Flacke, B. Fuks, L. Panizzi, H. Shao, Single production of vector-like quarks: the effects of large width, interference and NLO corrections. JHEP **08**, 107 (2021). https://doi.org/10.1007/JHEP08(2021)107. arXiv:2105.08745 [hep-ph]. [Erratum: JHEP **11**, 028 (2022)]
15. A. Buckley, J.M. Butterworth, L. Corpe, D. Huang, P. Sun, New sensitivity of current LHC measurements to vector-like quarks. SciPost Phys. **9**(5), 069 (2020). https://doi.org/10.21468/SciPostPhys.9.5.069. arXiv:2006.07172 [hep-ph]
16. X. Gong, C.X. Yue, Y.C. Guo, Search for vector-like bottom quark via Zb production at the LHC. Phys. Lett. B **793**, 175–180 (2019). https://doi.org/10.1016/j.physletb.2019.04.051. arXiv:1904.08206 [hep-ph]
17. D.H. Wang, L. Wu, M.C. Zhang, Hunting for top partner with a new signature at the LHC. Phys. Rev. D **103**(11), 115017 (2021). https://doi.org/10.1103/PhysRevD.103.115017. arXiv:2007.09722 [hep-ph]
18. B.F. Yang, X.L. Sima, S.Y. Wang, L.L. Shang, Single vectorlike top quark production in the tZ channel at high energy pp colliders. Phys. Rev. D **105**(9), 096010 (2022). https://doi.org/10.1103/PhysRevD.105.096010
19. J.Z. Han, S. Xu, H.Q. Song, Y.J. Wang, Single production of vectorlike B quarks decaying into bh at the CLIC. Nucl. Phys. B **985**, 116030 (2022). https://doi.org/10.1016/j.nuclphysb.2022.116030
20. L. Han, J.F. Shen, Search for single production of vector-like B quark decaying to bZ at future linear colliders. Eur. Phys. J. C **81**(5), 463 (2021). https://doi.org/10.1140/epjc/s10052-021-09245-y
21. L.L. Shang, C.P. Chen, S.Y. Wang, B.F. Yang, Single production of vector-like B quark decaying into bZ at future ep colliders. Nucl. Phys. B **984**, 115977 (2022). https://doi.org/10.1016/j.nuclphysb.2022.115977
22. G. Cacciapaglia, A. Carvalho, A. Deandrea, T. Flacke, B. Fuks, D. Majumder, L. Panizzi, H.-S. Shao, Next-to-leading-order predictions for single vector-like quark production at the LHC. Phys. Lett. B **793**, 206–211 (2019). https://doi.org/10.1016/j.physletb.2019.04.056. arXiv:1811.05055 [hep-ph]
23. A. Carvalho, S. Moretti, D. O'Brien, L. Panizzi, H. Prager, Single production of vectorlike quarks with large width at the Large Hadron Collider. Phys. Rev. D **98**(1), 015029 (2018). https://doi.org/10.1103/PhysRevD.98.015029. arXiv:1805.06402 [hep-ph]
24. A.E. Cárcamo Hernández, S.F. King, H. Lee, Z mediated flavor changing neutral currents with a fourth vectorlike family. Phys. Rev. D **105**(1), 015021 (2022). https://doi.org/10.1103/PhysRevD.105.015021. arXiv:2110.07630 [hep-ph]
25. A. Deandrea, A.M. Iyer, Vectorlike quarks and heavy colored bosons at the LHC. Phys. Rev. D **97**(5), 055002 (2018). https://doi.org/10.1103/PhysRevD.97.055002. arXiv:1710.01515 [hep-ph]
26. G. Cacciapaglia, A. Deandrea, N. Gaur, D. Harada, Y. Okada, L. Panizzi, The LHC potential of vector-like quark doublets. JHEP **11**, 055 (2018). https://doi.org/10.1007/JHEP11(2018)055. arXiv:1806.01024 [hep-ph]
27. G. Cacciapaglia, H. Cai, A. Carvalho, A. Deandrea, T. Flacke, B. Fuks, D. Majumder, H.-S. Shao, Probing vector-like quark models with Higgs-boson pair production. JHEP **07**, 005 (2017). https://doi.org/10.1007/JHEP07(2017)005. arXiv:1703.10614 [hep-ph]
28. S.J.D. King, S.F. King, S. Moretti, S.J. Rowley, Discovering the origin of Yukawa couplings at the LHC with a singlet Higgs and vector-like quarks. JHEP **21**, 144 (2020). https://doi.org/10.1007/JHEP05(2021)144. arXiv:2102.06091 [hep-ph]
29. J.-Z. Han, Y.-B. Liu, S.-Y. Xu, Pair production of the singlet vector-like B quark at the CLIC. Eur. Phys. J. C **84**(1), 61 (2024). https://doi.org/10.1140/epjc/s10052-023-12362-5. arXiv:2401.11423 [hep-ph]
30. A. Banerjee, V. Ellajosyula, L. Panizzi, Heavy vector-like quarks decaying to exotic scalars: a case study with triplets. JHEP **01**, 187 (2024). https://doi.org/10.1007/JHEP01(2024)187. arXiv:2311.17877 [hep-ph]
31. A.E.C. Hernández, S.F. King, H. Lee, Fermion mass hierarchies from vectorlike families with an extended 2HDM and a possible explanation for the electron and muon anomalous magnetic moments. Phys. Rev. D **103**(11), 115024 (2021). https://doi.org/10.1103/PhysRevD.103.115024. arXiv:2101.05819 [hep-ph]
32. A. Bhardwaj, K. Bhide, T. Mandal, S. Mitra, C. Neeraj, Discovery prospects of a vectorlike top partner decaying to a singlet boson. Phys. Rev. D **106**(7), 075024 (2022). https://doi.org/10.1103/PhysRevD.106.075024. arXiv:2204.09005 [hep-ph]
33. J. Bardhan, T. Mandal, S. Mitra, C. Neeraj, Machine learning-enhanced search for a vectorlike singlet B quark decaying to a singlet scalar or pseudoscalar. Phys. Rev. D **107**(11), 115001 (2023). https://doi.org/10.1103/PhysRevD.107.115001. arXiv:2212.02442 [hep-ph]
34. A. Bhardwaj, T. Mandal, S. Mitra, C. Neeraj, Roadmap to explore vectorlike quarks decaying to a new scalar or pseudoscalar. Phys. Rev. D **106**(9), 095014 (2022). https://doi.org/10.1103/PhysRevD.106.095014. arXiv:2203.13753 [hep-ph]
35. Y.-B. Liu, B. Hu, C.-Z. Li, Single production of vectorlike quarks with charge 5/3 at the 14 TeV LHC. arXiv:2402.01248 [hep-ph]
36. A.C. Canbay, O. Cakir, Investigating the single production of vectorlike quarks decaying into a top quark and W boson through hadronic channels at the HL-LHC. Phys. Rev. D **108**(9), 095006 (2023). https://doi.org/10.1103/PhysRevD.108.095006. arXiv:2307.12883 [hep-ph]
37. J.-Z. Han, S. Xu, W.-J. Mao, H.-Q. Song, Single production of vectorlike X quarks at the HL-LHC. Nucl. Phys. B **992**, 116235 (2023). https://doi.org/10.1016/j.nuclphysb.2023.116235
38. J.Z. Han, Y.B. Liu, L. Xing, S. Xu, Search for single production of vectorlike B-quarks at the LHC*. Chin. Phys. C **46**(10), 103103 (2022). https://doi.org/10.1088/1674-1137/ac79ab. arXiv:2208.06845 [hep-ph]
39. L. Han, L.-F. Du, Y.-B. Liu, Single production of vectorlike T quark at future high-energy linear e+e- collider. Phys. Rev. D **105**(11), 115032 (2022). https://doi.org/10.1103/PhysRevD.105.115032. arXiv:2206.06562 [hep-ph]
40. J.Z. Han, J. Yang, S. Xu, H.K. Wang, Search for single production of vector-like B quark via bZ channel at the HL-LHC. Nucl. Phys. B **975**, 115672 (2022). https://doi.org/10.1016/j.nuclphysb.2022.115672
41. J.-Z. Han, J. Yang, S. Xu, H.-K. Wang, Single production of vectorlike B quarks at the CLIC. Phys. Rev. D **105**(1), 015005 (2022). https://doi.org/10.1103/PhysRevD.105.015005. arXiv:2112.15044 [hep-ph]
42. X.-Y. Tian, L.-F. Du, Y.-B. Liu, Search for single production of vectorlike top partners through th channel at the HE-LHC and FCC-hh. Eur. Phys. J. C **81**(7), 594 (2021). https://doi.org/10.1140/epjc/s10052-021-09385-1
43. B. Yang, M. Wang, H. Bi, L. Shang, Single production of vectorlike T quark decaying into Wb at the LHC and the future pp colliders. Phys. Rev. D **103**(3), 036006 (2021). https://doi.org/10.1103/PhysRevD.103.036006

44. V. Cetinkaya, A. Ozansoy, V. Ari, O.M. Ozsimsek, O. Cakir, Single production of vectorlike Y quarks at the HL-LHC. Nucl. Phys. B **973**, 115580 (2021). https://doi.org/10.1016/j.nuclphysb.2021.115580. arXiv:2012.15308 [hep-ph]
45. H. Zhou, N. Liu, Probing a new decay of a vectorlike top partner mediated by a heavy Majorana neutrino via single production. Phys. Rev. D **101**(11), 115028 (2020). https://doi.org/10.1103/PhysRevD.101.115028. arXiv:2006.05296 [hep-ph]
46. Y.-B. Liu, Search for single production of the heavy vectorlike T quark with $T \to th$ and $h \to \gamma\gamma$ at the high-luminosity LHC. Phys. Rev. D **95**(3), 035013 (2017). https://doi.org/10.1103/PhysRevD.95.035013. arXiv:1612.05851 [hep-ph]
47. C.-H. Chen, T. Nomura, Single production of $X_{\pm 5/3}$ and $Y_{\mp 4/3}$ vectorlike quarks at the LHC. Phys. Rev. D **94**(3), 035001 (2016). https://doi.org/10.1103/PhysRevD.94.035001. arXiv:1603.05837 [hep-ph]
48. R. Barcelo, A. Carmona, M. Chala, M. Masip, J. Santiago, Single vectorlike quark production at the LHC. Nucl. Phys. B **857**, 172–184 (2012). https://doi.org/10.1016/j.nuclphysb.2011.12.012. arXiv:1110.5914 [hep-ph]
49. L. Shang, Y. Yan, S. Moretti, B. Yang, Single production of an exotic vector-like Y quark at future high energy pp colliders. arXiv:2401.00770 [hep-ph]
50. Y.-B. Liu, S. Moretti, Search for single production of a top quark partner via the $T \to th$ and $h \to WW^*$ channels at the LHC. Phys. Rev. D **100**(1), 015025 (2019). https://doi.org/10.1103/PhysRevD.100.015025. arXiv:1902.03022 [hep-ph]
51. C.M.S. Collaboration, A.M. Sirunyan et al., A search for bottom-type, vector-like quark pair production in a fully hadronic final state in proton-proton collisions at $\sqrt{s} = 13$ TeV. Phys. Rev. D **102**, 112004 (2020). https://doi.org/10.1103/PhysRevD.102.112004. arXiv:2008.09835 [hep-ex]
52. ATLAS Collaboration, G. Aad et al., Search for single vector-like B quark production and decay via $B \to bH(b\bar{b})$ in pp collisions at $\sqrt{s} = 13$ TeV with the ATLAS detector. arXiv:2308.02595 [hep-ex]
53. M. Buchkremer, G. Cacciapaglia, A. Deandrea, L. Panizzi, Model independent framework for searches of top partners. Nucl. Phys. B **876**, 376–417 (2013). https://doi.org/10.1016/j.nuclphysb.2013.08.010. arXiv:1305.4172 [hep-ph]
54. D. Guest, K. Cranmer, D. Whiteson, Deep learning and its application to LHC physics. Ann. Rev. Nucl. Part. Sci. **68**, 161–181 (2018). https://doi.org/10.1146/annurev-nucl-101917-021019. arXiv:1806.11484 [hep-ex]
55. A. Butter et al., The machine learning landscape of top taggers. SciPost Phys. **7**, 014 (2019). https://doi.org/10.21468/SciPostPhys.7.1.014. arXiv:1902.09914 [hep-ph]
56. M. Kagan, Image-Based Jet Analysis. arXiv:2012.09719 [physics.data-an]
57. C.W. Chiang, D. Shih, S.F. Wei, VBF vs. GGF Higgs with full-event deep learning: towards a decay-agnostic tagger. Phys. Rev. D **107**(1), 016014 (2023). https://doi.org/10.1103/PhysRevD.107.016014. arXiv:2209.05518 [hep-ph]
58. T. Chen, C. Guestrin, XGBoost: a scalable tree boosting system, in *Proceedings of the 22nd ACM SIGKDD International Conference on Knowledge Discovery and Data Mining, KDD '16* (Association for Computing Machinery, New York, 2016), pp. 785-794. https://doi.org/10.1145/2939672.2939785
59. D. Alvestad et al., Beyond cuts in small signal scenarios: enhanced sneutrino detectability using machine learning. Eur. Phys. J. C **83**(5), 379 (2023). https://doi.org/10.1140/epjc/s10052-023-11532-9. arXiv:2108.03125 [hep-ph]
60. F. Gianotti et al., Physics potential and experimental challenges of the LHC luminosity upgrade. Eur. Phys. J. C **39**, 293–333 (2005). https://doi.org/10.1140/epjc/s2004-02061-6. arXiv:hep-ph/0204087
61. A. Alloul, N.D. Christensen, C. Degrande, C. Duhr, B. Fuks, FeynRules 2.0—a complete toolbox for tree-level phenomenology. Comput. Phys. Commun. **185**, 2250–2300 (2014). https://doi.org/10.1016/j.cpc.2014.04.012. arXiv:1310.1921 [hep-ph]
62. Singlet b model (vlq), (2014). https://feynrules.irmp.ucl.ac.be/wiki/VLQ_bsingletvl. Accessed 2 Feb 2024
63. H.J. He, Y.P. Kuang, X.Y. Li, On the precise formulation of equivalence theorem. Phys. Rev. Lett. **69**, 2619–2622 (1992). https://doi.org/10.1103/PhysRevLett.69.2619
64. H.J. He, Y.P. Kuang, X.Y. Li, Further investigation on the precise formulation of the equivalence theorem. Phys. Rev. D **49**, 4842–4872 (1994). https://doi.org/10.1103/PhysRevD.49.4842
65. J. Alwall, R. Frederix, S. Frixione, V. Hirschi, F. Maltoni, O. Mattelaer, H.S. Shao, T. Stelzer, P. Torrielli, M. Zaro, The automated computation of tree-level and next-to-leading order differential cross sections, and their matching to parton shower simulations. JHEP **07**, 079 (2014). https://doi.org/10.1007/JHEP07(2014)079. arXiv:1405.0301 [hep-ph]
66. NNPDF Collaboration, R.D. Ball et al., Parton distributions from high-precision collider data. Eur. Phys. J. C **77**(10), 663 (2017). https://doi.org/10.1140/epjc/s10052-017-5199-5. arXiv:1706.00428 [hep-ph]
67. Particle Data Group Collaboration, R.L. Workman et al., Review of particle physics. PTEP **2022**, 083C01 (2022). https://doi.org/10.1093/ptep/ptac097
68. B. Belfatto, S. Trifinopoulos, Cabibbo angle anomalies and oblique corrections: the remarkable role of the vectorlike quark doublet. Phys. Rev. D **108**(3), 035022 (2023). https://doi.org/10.1103/PhysRevD.108.035022. arXiv:2302.14097 [hep-ph]
69. A. Crivellin, M. Kirk, T. Kitahara, F. Mescia, Global fit of modified quark couplings to EW gauge bosons and vector-like quarks in light of the Cabibbo angle anomaly. JHEP **03**, 234 (2023). https://doi.org/10.1007/JHEP03(2023)234. arXiv:2212.06862 [hep-ph]
70. S. Balaji, Asymmetry in flavour changing electromagnetic transitions of vector-like quarks. JHEP **05**, 015 (2022). https://doi.org/10.1007/JHEP05(2022)015. arXiv:2110.05473 [hep-ph]
71. G.C. Branco, J.T. Penedo, P.M.F. Pereira, M.N. Rebelo, J.I. Silva-Marcos, Addressing the CKM unitarity problem with a vector-like up quark. JHEP **07**, 099 (2021). https://doi.org/10.1007/JHEP07(2021)099. arXiv:2103.13409 [hep-ph]
72. D. Vatsyayan, A. Kundu, Constraints on the quark mixing matrix with vector-like quarks. Nucl. Phys. B **960**, 115208 (2020). https://doi.org/10.1016/j.nuclphysb.2020.115208. arXiv:2007.02327 [hep-ph]
73. F.J. Botella, G.C. Branco, M. Nebot, M.N. Rebelo, J.I. Silva-Marcos, Vector-like quarks at the origin of light quark masses and mixing. Eur. Phys. J. C **77**(6), 408 (2017). https://doi.org/10.1140/epjc/s10052-017-4933-3. arXiv:1610.03018 [hep-ph]
74. K. Ishiwata, Z. Ligeti, M.B. Wise, New vector-like fermions and flavor physics. JHEP **10**, 027 (2015). https://doi.org/10.1007/JHEP10(2015)027. arXiv:1506.03484 [hep-ph]
75. A.K. Alok, S. Banerjee, D. Kumar, S.U. Sankar, D. London, New-physics signals of a model with a vector-singlet up-type quark. Phys. Rev. D **92**, 013002 (2015). https://doi.org/10.1103/PhysRevD.92.013002. arXiv:1504.00517 [hep-ph]
76. G. Cacciapaglia, A. Deandrea, N. Gaur, D. Harada, Y. Okada, L. Panizzi, Interplay of vector-like top partner multiplets in a realistic mixing set-up. JHEP **09**, 012 (2015). https://doi.org/10.1007/JHEP09(2015)012. arXiv:1502.00370 [hep-ph]
77. F.J. Botella, G.C. Branco, M. Nebot, The hunt for new physics in the flavour sector with up vector-like quarks. JHEP **12**, 040 (2012). https://doi.org/10.1007/JHEP12(2012)040. arXiv:1207.4440 [hep-ph]
78. G. Cacciapaglia, A. Deandrea, D. Harada, Y. Okada, Bounds and decays of new heavy vector-like top partners. JHEP **11**, 159 (2010).

https://doi.org/10.1007/JHEP11(2010)159. arXiv:1007.2933 [hep-ph]
79. J.M. Campbell, R.K. Ellis, F. Maltoni, S. Willenbrock, Production of a Z boson and two jets with one heavy-quark tag. Phys. Rev. D **73**, 054007 (2006). https://doi.org/10.1103/PhysRevD.77.019903. arXiv:hep-ph/0510362. [Erratum: Phys. Rev. D 77, 019903 (2008)]
80. J.M. Campbell, R.K. Ellis, An update on vector boson pair production at hadron colliders. Phys. Rev. D **60**, 113006 (1999). https://doi.org/10.1103/PhysRevD.60.113006. arXiv:hep-ph/9905386
81. A. Alloul, N.D. Christensen, C. Degrande, C. Duhr, B. Fuks, FeynRules 2.0—a complete toolbox for tree-level phenomenology. Comput. Phys. Commun. **185**, 2250–2300 (2014). https://doi.org/10.1016/j.cpc.2014.04.012. arXiv:1310.1921 [hep-ph]
82. C. Bierlich et al., A comprehensive guide to the physics and usage of PYTHIA 8.3. arXiv:2203.11601 [hep-ph]
83. DELPHES 3 Collaboration, J. de Favereau, C. Delaere, P. Demin, A. Giammanco, V. Lemaître, A. Mertens, M. Selvaggi, DELPHES 3, a modular framework for fast simulation of a generic collider experiment. JHEP **02**, 057 (2014). https://doi.org/10.1007/JHEP02(2014)057. arXiv:1307.6346 [hep-ex]
84. CERN Collaboration, M. Selvaggi, Delphes cards for LHC Run-III, and HL-LHC (2017). https://github.com/delphes/delphes/blob/master/cards/delphes_card_HLLHC.tcl. Accessed 25 Feb 2024
85. M. Cacciari, G.P. Salam, G. Soyez, FastJet user manual. Eur. Phys. J. C **72**, 1896 (2012). https://doi.org/10.1140/epjc/s10052-012-1896-2. arXiv:1111.6097 [hep-ph]
86. M. Cacciari, G.P. Salam, Dispelling the N^3 myth for the k_t jet-finder. Phys. Lett. B **641**, 57–61 (2006). https://doi.org/10.1016/j.physletb.2006.08.037. arXiv:hep-ph/0512210
87. E. Conte, B. Fuks, G. Serret, MadAnalysis 5, a user-friendly framework for collider phenomenology. Comput. Phys. Commun. **184**, 222–256 (2013). https://doi.org/10.1016/j.cpc.2012.09.009. arXiv:1206.1599 [hep-ph]
88. L.L. Shang, Y. Zhang, EasyScan_HEP: a tool for connecting programs to scan the parameter space of physics models. arXiv:2304.03636 [hep-ph]
89. E. Burns, W. Fisher, Testing the approximations described in 'Asymptotic formulae for likelihood-based tests of new physics'. arXiv:1110.5002 [hep-ex]
90. T. Fawcett, An introduction to roc analysis. Pattern Recognit. Lett. **27**(8), 861–874 (2006). https://doi.org/10.1016/j.patrec.2005.10.010
91. J. Snoek, H. Larochelle, R.P. Adams, Practical Bayesian Optimization of Machine Learning Algorithms. arXiv:1206.2944 [stat.ML]